Journal of Alloys and Compounds 509 (2011) 1777–1780

Contents lists available at ScienceDirect

Journal of Alloys and Compounds

journal homepage: www.elsevier.com/locate/jallcom

Preparation and characterization of CNTs–$SrFe_{12}O_{19}$ composites

Li Qiao-ling[a,*], Ye Yun[b], Zhao De-xu[a], Zhang Wei[a], Zhang Yan[a]

[a] Department of chemistry, North University of China, Taiyuan 030051, China
[b] National Key Laboratory For Electronic Measurement Technology, School of Materials Science and Engineering, North University of China, Taiyuan 030051, China

ARTICLE INFO

Article history:
Received 19 May 2010
Received in revised form 3 October 2010
Accepted 10 October 2010
Available online 23 October 2010

Keywords:
Carbon nanotubes
Nanocomposites
Aggregation
Formation mechanism

ABSTRACT

$SrFe_{12}O_{19}$ nanoparticles are adsorbed alongside the CNTs via in situ sol–gel method. The crystal structure and morphology of the as-synthesized sample are characterized by X-ray diffraction pattern (XRD), transmission electron microscope (TEM). The results shown that a large number of the high purity $SrFe_{12}O_{19}$ nanocrystallites are decorated on the sidewalls of the CNTs, and these nanocrystallites aggregated around the CNTs templates form compact cladding. The probable formation mechanism of the nanocomposites is also investigated based on the experimental results.

1. Introduction

Since the discovery of carbon nanotubes (CNTs), polymer-based composites including carbon nanotubes have attracted considerable attention in the research and industrial communities, due to their good electrical conductivity, high stiffness and high strength at relatively low CNTs content [1–6]. Currently, three methods are commonly used to introduce CNTs into polymers: (1) solution mixing or film casting of suspensions of CNTs in dissolved polymer [7], (2) in situ polymerization of CNT–polymer monomer mixture [8], and (3) mechanically melt mixing of CNTs with polymers [9].

Besides that, CNTs can also form composites with many inorganic materials. For examples, Ma et al. [10] have prepared CNT–SiC composites by hot-pressing the mixture of large multiwall carbon nanotubes (MWNTs: 30–40 nm in diameter) and SiC powder. Novel composite powders such as CNT–Fe/Co–$MgAl_2O_4$ and CNT–Co–MgO have been synthesized [11–14]. Peigney et al. have produced the CNT–Fe–Al_2O_3 powders [15] in which the CNTs are very homogeneously dispersed between the metal oxide grains. These CNT–metal oxide composites are electrical conductors owing to the percolation of the carbon nanotubes. SiO_x coated CNTs [16] have also been fabricated through a sol–gel technique at room temperature. Multi-walled carbon nanotube (MWNT)-based metal oxide composites [17] are prepared by an impregnation method using organometallic compounds as precursor. Chen et al. [18] obtained SnO–CNT composites by a sol–gel method as anode active material for lithium-ion batteries. Han and Zettl [19] have coated single-walled carbon nanotubes with a thin SnO_2 layer (about 4 nm) by a chemical-solution route. The MWNTs–SnO_2 composites fabricated by a new and simple one-step wet chemical method [20] have also been reported recently.

Here we produced CNTs–$SrFe_{12}O_{19}$ composites by the in situ sol–gel method in which the formation of $SrFe_{12}O_{19}$ and its compounding with CNTs happened almost simultaneously. The as produced composites are examined by transmission electron microscopy (TEM). Results showed that purified CNTs are well coated with $SrFe_{12}O_{19}$. And the probable formation mechanism of the composites is investigated based on the experimental results.

2. Experimental

2.1. Oxidative modification of CNTs

The pristine CNTs are first roasted at 520 °C for 2 h in a quartz tube furnace. Next, they are dispersed into concentrated nitration mixture (VH_2SO_4:$VHNO_3$ = 3:1) at 80 °C, with constant stirring for 6 h. Subsequently, the solution is treated with an ultrasonicator for 6 h. Finally, the solution is diluted with distilled water and rinsed several times until the pH value reached neutral. The resulting CNTs are separated from the solution by filtration and dried in a vacuum oven at 60 °C for further use.

2.2. Synthesis of CNTs–$SrFe_{12}O_{19}$ composites

CNTs–$SrFe_{12}O_{19}$ composites are prepared by using absorbent cotton as a template by the in situ sol–gel method. The detailed process could be described as follows. $Sr(NO_3)_2$ and $Fe(NO_3)_3{\cdot}9H_2O$ (the mole ratio of Fe^{3+}/Sr^{2+} is 11.5) are dissolved in 200 ml deionized water, and mixed with 2% (quality score) modified CNTs. Next, citric acid (the mole ratio of citric acid/metal ion is 1:1) is added to the above-mentioned mixture. The pH value is adjusted to 6 by adding $NH_3{\cdot}H_2O$ after the solution is stirred homogeneously; it is treated with an ultrasonicator for 30 min. Subsequently, the solutions are treated at 80 °C for 6 h, 18 h (including stewing for 6 h), 30 h (including stewing for 12 h) respectively, and the other solutions are

* Corresponding author at: Department of chemistry, North University of China, Taiyuan 030051, China. Tel.: +86 035 139 23197; fax: +86 035 139 22152.
E-mail address: qiaolingl@163.com (Q.-l. Li).

0925-8388/$ – see front matter © 2010 Elsevier B.V. All rights reserved.
doi:10.1016/j.jallcom.2010.10.038

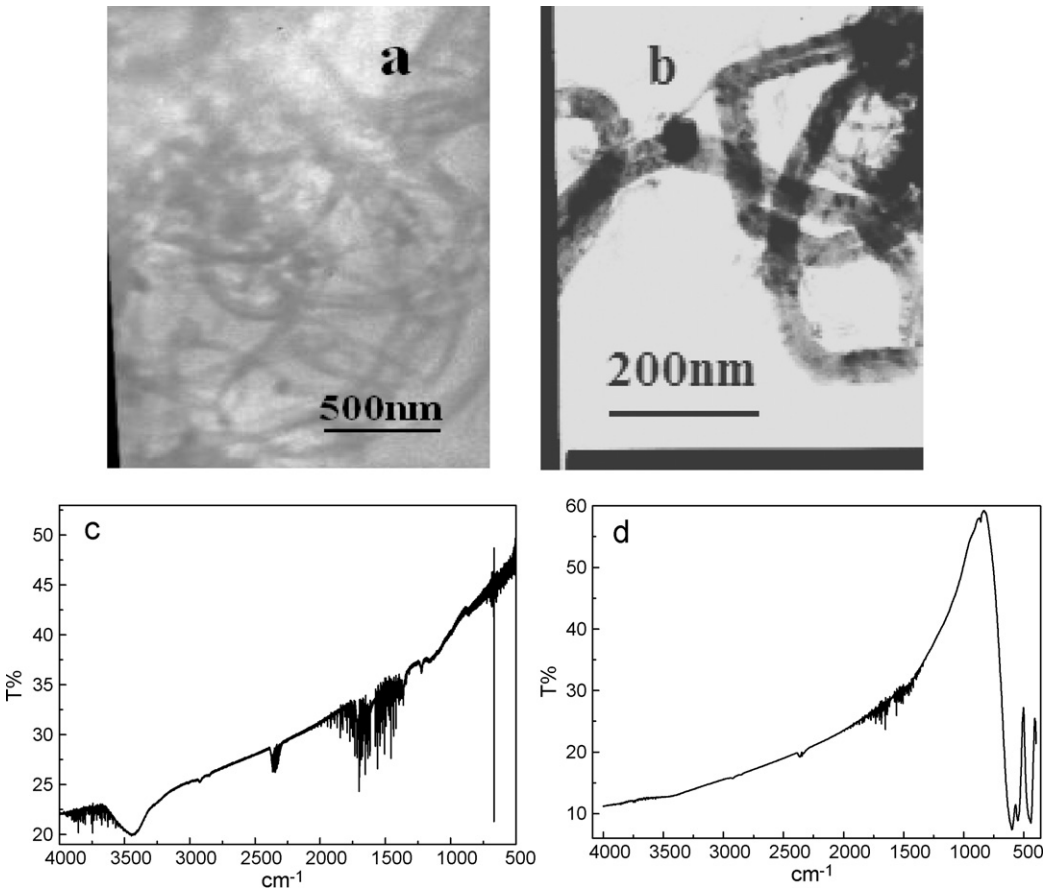

Fig. 1. TEM images of original CNTs (a) and after oxidation treatment by nitration mixture (b) FT-IR spectra of purified CNTs (c) and CNTs–$SrFe_{12}O_{19}$ (d).

treated at 50 °C for 6 h, 18 h (including stewing for 6 h), 30 h (including stewing for 12 h) respectively, the remaining solution is dipped by the absorbent cotton. They are further dried for 12 h at 80 °C. Finally, all the dried gels are then calcined under 850 °C for 2 h to obtain CNTs–$SrFe_{12}O_{19}$ samples, and they are recorded as a, b, c, a_1, b_1, c_1.

2.3. Characterization

The crystalline structure of the samples is determined by α D/max-A diffractometer (Cu Kα radiation, λ = 0.154056 nm) studies. The transmission electron microscope (TEM, H-800) is used to examine the structures and to determine further details of the nanocomposites.

3. Results and discussion

FT-IR spectra of purified CNTs (c) and CNTs–$SrFe_{12}O_{19}$ (d).

It is well-known that most as produced CNTs contain some impurities such as amorphous carbon, fullerenes and catalyst particles, which are a serious impediment for CNTs to be directly used as functional filler in composites. Therefore, oxidative modification of carbon nanotubes is necessary. As can be seen in Fig. 1(a), the pristine CNTs are long and curve; they are tangled together under electrostatic force. Fig. 1(b) shows the TEM image of purified CNTs in which the long interwined CNTs with a diameter of about 30 nm are very clean and almost all impurities had been removed. Thus the purification for CNTs is effective. The oxidation treatment can improve the wetting effect between the CNTs and the polymer, it can also make the surface of CNTs introduce the functional groups which can react with the polymer matrix, so as to further enhance the cementation between them [21,22].

Fig. 1(c) shows the FTIR spectra of modified CNTs, the peak at 3447 cm^{-1} is due to –OH group (due to oxidation with H_2SO_4 and HNO_3), One can see this peak is broadened in Fig. 1(c). As the peak at 2924 cm^{-1} are assigned to the asymmetrical stretching of methylene (–CH_2–). The peak at 2390 cm^{-1} is assigned to the bending vibration of the adsorbed molecular water. The peak at 673 cm^{-1} may be due to the plane bending vibration of the C–H bond. 1225 cm^{-1} corresponding to the characteristic absorption peak of –SO_4^-, Hydrophilic –SO_4^- negative electricity group spread into the surrounding solvent water molecules, the van der Waals force between CNTs was overcome by electrostatic repulsion interaction of negative electricity group, and the reunion between CNTs was broken [23], which created favorable conditions for adsorption with strontium ferrite nanoparticles. In Fig. 1(d), there are peaks at about 598 cm^{-1}, 551 cm^{-1} and 440 cm^{-1}, respectively. They are all located in the region between 400 cm^{-1} and 800 cm^{-1}. Previous reports [24] have shown that they are the characteristic peaks of $SrFe_{12}O_{19}$.

From the TEM images in Fig. 2, which can be found that with the increasing of reaction and deposition time, $SrFe_{12}O_{19}$ nanoparticles coated on the surface of CNTs increasingly dense and smooth, and radial size of the CNTs–$SrFe_{12}O_{19}$ composites is also smaller, which indicates that reaction time plays an important role in the coating effect. And with the lengthening of the reaction and deposition time, more $SrFe_{12}O_{19}$ nanoparticles can be aggregated to the surface of CNTs, and the spacing among $SrFe_{12}O_{19}$ particles will be getting smaller and smaller. Therefore, the surface of CNTs is more smooth and coated more completely. As for the aggregation of nanocrystallites, it has been proposed that the aggregation growth will initiate when the repulsive interactions are not large enough to block their access due to Brownian motion and van der Waals attraction [25,26]. Currently, the main driving force for aggregation of nanocrystals is attributed to the tendency to decrease the high surface energy. In our case, dipolar interactions between the

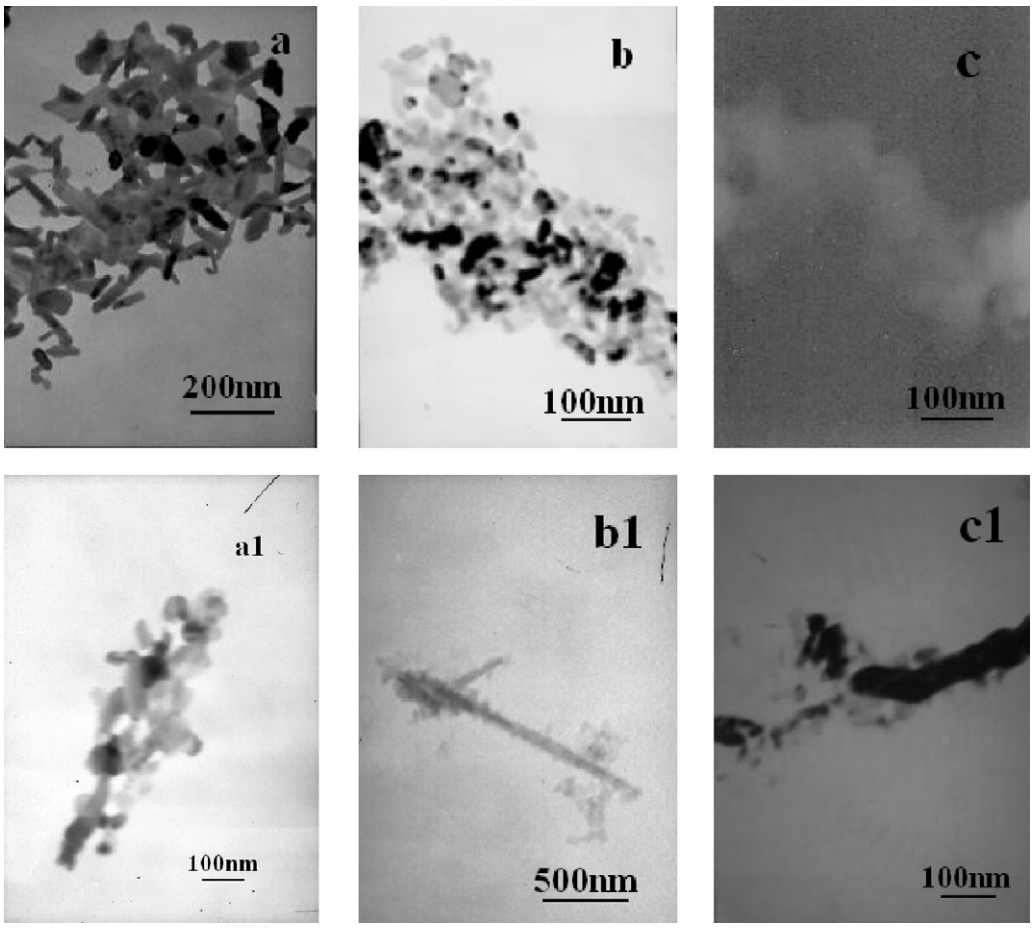

Fig. 2. TEM images of CNTs–$SrFe_{12}O_{19}$ (a, b, c. $T = 80\,^{\circ}C$) and (a1, b1, c1. $T = 50\,^{\circ}C$).

magnetite nanoparticles are also contributive to their aggregation [27].

The aggregation process may be divided into three steps: 1. The irregular adsorption at the molecular level; 2. The rearrangement between $SrFe_{12}O_{19}$ particles; 3. The "close packing" and growing up of the $SrFe_{12}O_{19}$ particles. As shown in Fig. 3:

In addition, the stability of CNTs is greatly enhanced after ultrasonic oscillation. This is because in ultrasonic field, the "ultrasonic cavitation bubbles" generated by frequency ultrasonic wave release tremendous energy when they exploded, producing local high temperature, pressure environment and internal jet which had a strong impact force. This cavitation, making CNTs fracture into smaller short-tubes from their modified defects, plays shear effect on their reunion and is conducive to the formation of small particles [28]. The active groups on the surface of CNTs greatly increase their dispersion in the solution, and $SrFe_{12}O_{19}$ nanoparticles adsorb on the surface of CNTs as the role of active groups.

In Fig. 2(a), (b), (c), the number of $SrFe_{12}O_{19}$ particles is larger than that of Fig. 2(a1), (b1), (c1), but the particles size is smaller than the latter. It shows that the temperatures also have a great effect on the preparation of samples. This is mainly because: The preparation of nanoparticles includes two processes of nucleation and growth, and nucleation is rapid and transient, but the growth of crystal is relatively slow. Crystal nucleation rate depends on the temperature of the reaction. The faster the nucleation rate is, the nuclei are more symmetrical. And at this moment the nucleation rate is much greater than the growth rate. The lower the reaction temperature is, the reaction time is longer. But with the ongoing of the reaction, austenitic maturation will occur between the nanoparticles. The higher surface energy of the smaller nanoparticles dissolve and re-grow to larger nanoparticles [29], the particles size of the latter is larger.

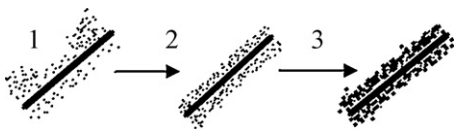

Fig. 3. Schematic diagram of CNTs–$SrFe_{12}O_{19}$ sample preparation process.

It is confirmed that the heating rate has significant influence on the final product. In a comparable experiment, the heating rate is decreased to $50\,^{\circ}C$. It is well-known that the higher temperature of reaction facilitates higher nucleation rates [30]. As a result of the enhanced nucleation rate, more nuclei are formed at the initial stage. And some nuclei will grow into separated nanoparticles before they can attach to the CNTs. These nanoparticles have much high surface energy and are preferentially attached onto the surface of CNTs from automatically. The tiny nanoparticles will then serve as the nuclei for the growth of magnetite nanoparticles [31,32].

Fig. 4 shows the XRD patterns of the as-prepared product. It is found that the peaks in the two graphs are basically the same. The analysis result indicates that the product is a mixture of two phases: CNTs and $SrFe_{12}O_{19}$ (JCPDS card No. 24-1207). And no peaks corresponding to impurities are detected. The positions and relative intensities of these non-MWCNTs related peaks match well with the (1 1 0), (1 0 7), (1 1 4), (2 0 3), (2 0 5), and (2 0 6) planes of the standard XRD data for the M-type structure of magneto-plumbite

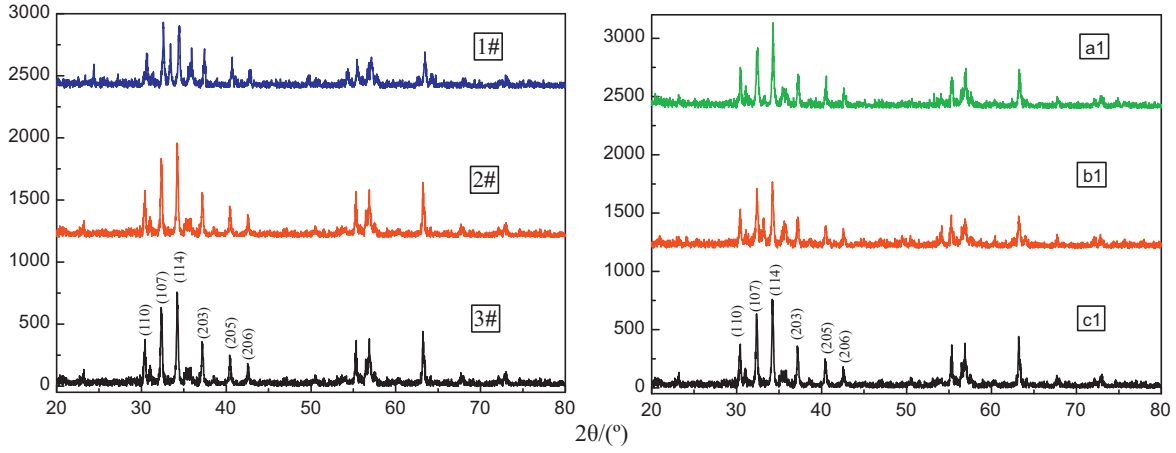

Fig. 4. XRD patterns of CNTs–$SrFe_{12}O_{19}$ (a, b, c. $T = 80\,^{\circ}C$) and (a1, b1, c1. $T = 50\,^{\circ}C$).

ferrite. The weak diffraction peaks at $2\theta = 26.8^{\circ}$ and $2\theta = 54.4^{\circ}$ are the typical peaks of CNTs and can be indexed to the (0 0 2) and (0 0 4) reflections of CNTs [30], but they only appear in Fig. 4(1). It indicates that the CNTs are completely coated by $SrFe_{12}O_{19}$ nanoparticles in Fig. 4(2), (3) instead of Fig. 4(1). This is mainly because that with the reaction time increasing, more $SrFe_{12}O_{19}$ nanoparticles are assembled to the surface of CNTs, and they are coated more complete with $SrFe_{12}O_{19}$ nanoparticles. Therefore, no characteristic peaks of CNTs are appeared in Fig. 4(2), (3). In Fig. 4(a1), (b1), (c1), though the diffraction peak of CNTs at $2\theta = 26.8^{\circ}$ does not appear, the peak at $2\theta = 54.4^{\circ}$ is emerged. This indicates that the reaction temperature has a certain impact on the coating effect.

4. Conclusions

In summary, the in situ sol–gel method has been used to successfully synthesize $SrFe_{12}O_{19}$/CNTs nanocomposites. This approach develops a simple, efficient, and scalable route to fabricate the tiny magnetic $SrFe_{12}O_{19}$ nanocrystals aggregating around the sidewalls of CNTs. Based on the experimental results, it is found that with the increase of standing time and reaction temperature, the surface of the sample is more smooth and is covered more completely. When ultrasonic treatment is for 30 min, the reaction time and temperature are 30 h (including stewing for 12 h) and 80 °C, respectively. The coating on the CNTs with $SrFe_{12}O_{19}$ nanoparticles is the best, which will help $SrFe_{12}O_{19}$ and CNTs complement each other's advantages and achieve the organic integration of their magnetic and electrical properties. The nano-composite has a great potential application in the efficient absorption of the electromagnetic wave.

Acknowledgements

The authors acknowledge the North University of China for the support given for carrying out this study under projects from the National Natural Science Fund (20871108) and the projects of qualified personnel plan of the Nation and Province.

References

[1] M.S.P. Shaffer, A.H. Windle, Advanced Materials 11 (1999) 937–941.
[2] R. Andrews, D. Jacques, M. Minot, T. Rantell, Macromolecular Materials and Engineering 287 (2002) 395–403.
[3] C.A. Cooper, D. Ravich, D. Lips, J. Mayer, H.D. Wagner, Composites Science and Technology 62 (2002) 1105–1112.
[4] R. Haggenmueller, H.H. Gommans, A.G. Rinzler, J.E. Fischer, K.I. Winey, Chemical Physics Letters 330 (2000) 219–225.
[5] Z. Jin, K.P. Pramoda, G. Xu, S.H. Goh, Chemical Physics Letters 337 (2001) 43–47.
[6] J. Sandler, M.S.P. Shaffer, T. Prasse, W. Bauhofer, K. Schulte, A.H. Windle, Polymer 40 (1999) 5967–5971.
[7] R. Haggenmuller, H.H. Gonmas, A.G. Rinzler, J.E. Fischer, K.I. Winey, Chemical Physics Letters 330 (2000) 219–225.
[8] Z.J. Jia, Z.Y. Wang, C.L. Xu, J. Liang, B.Q. Wei, D.H. Wu, S.W. Zhu, Materials Science & Engineering, A, Structural Materials: Properties, Microstructure and Processing 271 (1999) 395–400.
[9] J.X. Jin, K.P. Pramoda, S.H. Goh, G.Q. Xu, Materials Research Bulletin 37 (2002) 271–278.
[10] R.Z. Ma, J. Wu, B.Q. Wei, J. Liang, D.H. Wu, Journal of Materials Science 33 (1998) 5243–5246.
[11] A. Govindaraj, E. Flahaut, Ch. Laurent, A. Peigney, A. Rousset, C.N.R. Rao, Journal of Materials Research 14 (1999) 2567–2576.
[12] E. Flahaut, A. Govindaraj, A. Peigney, Ch. Laurent, A. Rousset, C.N.R. Rao, Chemical Physics Letters 300 (1999) 236–242.
[13] P. Coquay, E. DeGrave, R.E. Vandenberghe, C. Dauwe, E. Flahaut, Ch. Laurent, A. Peigney, A. Rousset, Acta Materialia 48 (2000) 3015–3023.
[14] E. Flahaut, A. Peigney, Ch. Laurent, A. Rousset, Journal of Materials Chemistry 10 (2000) 249–252.
[15] E. Flahaut, A. Peigney, Ch. Laurent, Ch. Marlière, F. Chastel, A. Rousset, Acta Materialia 48 (2000) 3803–3812.
[16] T. Seeger, Ph. Redlith, N. Grobert, M. Terrones, D.R.M. Walton, H.W. Kroto, M. Rühle, Chemical Physics Letters 339 (2001) 41–46.
[17] K. Hernadi, E. Ljubovic, J.W. Seo, L. Forró, Acta Materialia 51 (2003) 1447–1452.
[18] M.H. Chen, Z.C. Huang, G.T. Wu, G.M. Zhu, J.K. You, Z.G. Lin, Materials Research Bulletin 38 (2003) 831–836.
[19] W.Q. Han, A. Zettl, Nano Letters 3 (2003) 681–683.
[20] L.P. Zhao, L. Gao, Carbon 42 (2004) 1858–1861.
[21] Li Chen, Bai-Lan Zhang, Mei-Zhen Qu, et al., Powder Technology 154 (2005) 70–72.
[22] Yu-sheng Tang, Jun-wei Gu, Journal of Xi'an Shiyou University (Natural Science Edition) 24 (1) (2009) 67–71.
[23] L.U. Zhi-Hua, S.U.N. Kang-Ning, S.U.N. Xiao-Ning, et al., Journal of Inorganic Materials 22 (6) (2007) 1127–1130.
[24] Y.W. Du, Ferrite, Jiangsu Science and Technology Press, Nanjing, 1995.
[25] L.P. Zhao, L. Gao, Carbon 42 (2004) 1858.
[26] J.F. Banfield, S.A. Welch, H. Zhang, T.T. Ebert, R.L. Penn, Science 289 (2000) 751.
[27] Qi Zhang, Meifang Zhu, Qinghong Zhang, et al., Materials Chemistry and Physics 116 (2009) 658–662.
[28] Wen-liang Wang, Dong-sheng Li, Xiang-yang Hou, et al., Chemical Research and Application 13 (2) (2001) 157–159.
[29] Ji Tian-hao, Sun Jia-yue, Du Hai-yan, Dispersed Inorganic Nanoparticles—Preparation, Assembly and Application[M], Science Press, Beijing, 2009.
[30] H. Zhang, N. Du, P. Wu, B. Chen, D. Yang, Nanotechnology 19 (2008) 315604.
[31] Haitao Wang, Lili Cao, Shancheng Yan, et al., Materials Science and Engineering B 12142 (2009) 1–4.
[32] V. Nandwana, K.E. Elkins, N. Poudyal, G.S. Chaubey, K. Yano, J.P. Liu, Journal of Physical Chemistry C111 (2007) 4185–4189.